Environmentally transmitted disease: Stage structured infectious-propagule patches

November 26, 2016

Thomas Caraco[1,⋆] and Wendy C. Turner[1,†]

1. *Department of Biological Sciences, University at Albany, Albany NY 12222, USA*

⋆e-mail: tcaraco@albany.edu;
†Corresponding author, e-mail: wcturner@albany.edu

Abstract. First draft; working paper.

Keywords: free-living pathogen, host self-regulation, obligate killer, temporary immunity, virulence structure

1 Introduction

A number of important pathogens are transmitted through the physical environment; some have significance for wildlife conservation [Breban et al. 2010, Turner et al. 2013], and others infect human or agricultural hosts [Turner et al. 2006, Moore et al. 2014]. Environmental transmission, by definition, requires that the pathogen persist outside of host tissues, and many such pathogens have a free-living, infectious form capable of lengthy survival in the abiotic environment [Dwyer 1992, Godfray et al. 1997]. A persistent free-living stage can maintain the pathogen population through periods of low host density [Walther and Ewald 2004, Caraco and Wang 2008], and may relax epidemiological constraints on the evolution of virulence [Gandon 1998, Day 2002, Cressler et al. 2015].

Models for the evolutionary ecology of environmentally transmitted disease usually assume that a free-living pathogen, when released from an infected host, enters a homogeneously mixed pool. Within the pool, all pathogen particles (of a given strain) have the same longevity, the same rate of contacting hosts, and the same infectiousness upon contact [Alizon and Michalakis 2015]. That is, theory for disease transmission through the abiotic environment generally assumes that pathogens lack ecological or demographic structure. But, for many free-living pathogens, host contacts occur heterogeneously in space or time [Duryea et al. 1999, Roche et al. 2011, Caraco et al. 2016]. A consequence of this heterogeneity, upon which our study rests, is that infectious contacts with a free-living pathogen may often be structured with respect to both transmission and virulence.

Spatial clustering of environmental transmission commonly occurs when a pathogen must kill its current host to infect another; most obligate killers release infectious propagules only at the demise of diseased hosts [Ebert and Herre 1996]. For example, polyhedrosis virus kills moth larvae, and then viral particles are deposited on the leaf where the larva died. Subsequent infection occurs when another larva feeds on the same leaf

[Dwyer 1994, Reeson et al. 2000]. *Bacillus anthracis*, an obligate killer, has been studied in wildlife, particularly the plains zebra (*Equus quagga*). Infected herbivores may die a few days after exposure to the pathogen [Bagamian et al. 2013]. Carcasses exsanguinate, producing localized patches of anthrax spores. Nutrients from a carcass generate a local pulse of plant growth, which attracts herbivores to the infectious patch [Turner et al. 2014]. Patches can persist for a decade [Turnbull 2008], but spore density within a given patch declines with time [Turner et al. 2016], and the local vegetation returns to its initial state within a few years. The decline in spore density implies that exposure at an older patch is less likely to produce a fatal infection. Moreover, exposure to a smaller *B. anthracis* dose may induce an immune response [Rijks 1999, Cizauskas et al. 2014a], plausibly reducing an herbivore‘s susceptibility to subsequent infection [Cizauskas et al. 2014b]. That is, populations of some free-living pathogens may include more recent infectious patches that kill, and older patches that "vaccinate."

1.1 Organization

We develop some novel predictions by analyzing a host-pathogen ecology where patches of infectious propagules are structured with respect to transmission, virulence, and persistence. The plains zebra-*Bacillus anthracis* interaction [Gasaway et al. 1996, Turner et al. 2014] suggests some model details. But the addition of population structure to models of environmentally transmitted infections has far more general implications.

We organize the paper as follows. Section 2 develops a model in which seasonality separates host intraspecific competition from infection and disease. Coupling seasonal processes yields a dynamics for susceptible and resistant hosts, and for a stage-structured population of infectious patches. Section 3 analyzes disease-free growth of the host population, and derives a condition for pathogen invasion. Section 4 lists the fixed-point

endemic equilibria, which we use to study consequences of the pathogen's stage structure. Sections 5 through 7 present the main results; we consider pathogen patches structured by (1) infectious-encounter probabilities, by (2) the probability that an infection kills the host, and by (3) patch survival probabilities. We equate greater patch structure with increased between-stage heterogeneity in these traits, and compare numbers of hosts and patches to results of a stage-averaged, unstructured model. The Discussion summarizes our focal message:

2 Model

We model an annual cycle of wet and dry seasons [Havarua et al. 2014]. During the wet season, hosts experience infectious contacts with the free-living pathogen, some of which lead to fatal disease. Carcasses resulting from mortal infections become new pathogen patches the following year [Turner et al. 2013]. During the dry season, the herbivorous hosts compete for limited resources, so that their reproduction exhibits density dependence. Infectious patches may decay as a consequence of abiotic conditions during the dry season, and a fraction of highly infectious patches transition to a less infectious stage.

Year t begins at the start of a dry season. S_t represents the number of susceptible hosts, and R_t is the number of (partially) resistant hosts, entering the dry season. Resistance implies that the individual was exposed to the pathogen during the previous wet season, but recovered (or seroconverted) and retains some adaptive immunity. $P_{x,t}$ is the number of infectious patches at the start the dry season; $x = 1, 2$. Table 1 lists the state variables and model parameters.

Symbols	Definitions
S_t	Number of susceptible hosts, dry season, time t
R_t	Number of resistant hosts, dry season, time t
σ_t	Number of susceptible hosts entering wet season, time t
ρ_t	Number of resistant hosts entering wet season, time t
g	Proportional survival among hosts, dry season
γ	Proportional loss of resistance among R_t hosts
λ	Host natality
μ	Scales density-dependence of host natality
$P_{x,t}$	Number of stage-x infectious patches, dry season, time t; $x = 1, 2$
$\pi_{x,t}$	Number of stage-x infectious patches entering wet season, time t
ξ_x	Probability that a stage-x patch persists through dry season
q_{12}	Frequency of stage-1 to stage-2 transition among persisting $P_{1,t}$
β_x	Infectiousness of each stage-x patch; integrates encounter rate and chance of infection
$\nu_{\sigma,x}$	Disease-mortality probability for susceptibles infected at a stage-x patch
$\nu_{\rho,x}$	Disease-mortality probability for resistant hosts infected at a stage-x patch
θ_t	$\beta_1\pi_{1,t}/\left(\beta_1\pi_{1,t} + \beta_2\pi_{2,t}\right)$
$\mathbf{H_t}$	$[\theta_t,\ 1-\theta_t]$
$\mathbf{V}_\sigma$	$[\nu_{\sigma,1},\ \nu_{\sigma,2}]$
$\mathbf{Z}_\sigma$	$[1-\nu_{\sigma,1},\ 1-\nu_{\sigma,2}]$
$\mathbf{V}_\rho$	$[\nu_{\rho,1},\ \nu_{\rho,2}]$
$\mathbf{Z}_\rho$	$[1-\nu_{\rho,1},\ 1-\nu_{\rho,2}]$

Table 1: Definitions of model variables and symbols. Top: host population; middle: structured patches; bottom: vector-valued parameters.

2.1 Host reproduction, patch decay

During the dry season the number of susceptible hosts changes through non-disease mortality and loss of immunity among resistant hosts. A birth pulse at the beginning of the wet season [Gasaway et al. 1996] increases the number of susceptibles; all newborns enter the susceptible class. Collecting these changes, a total of σ_t susceptible hosts may be exposed to infection during the wet season:

$$\sigma_t = g(S_t + \gamma R_t) + \lambda(S_t + R_t)e^{-\mu(S_t+R_t)} \tag{1}$$

g is the fraction of all hosts $(S_t + R_t)$ that survive the dry season; $0 < g < 1$. γ is the proportion of the surviving R_t hosts that lose resistance and return to the susceptible class.

λ is the finite rate of increase, and host self-regulation has a Ricker form
78 [Avilés 1999, Trainor and Caraco 2006]. Density-dependence is a function of the number of hosts alive at the start of the dry season; the strength of self-regulation increases with μ.

80 The number of resistant hosts changes during the dry season through mortality and loss of resistance. Then ρ_t resistant hosts enter the wet season: $\rho_t = g(1-\gamma)R_t$. If η_t is the total
82 number of hosts that may be exposed to infection during the wet season, then $\eta_t = (S_t + R_t)\left[g + \lambda e^{-\mu(S_t+R_t)}\right]$.

84 The $P_{x,t}$ also change during the dry season; some patches decay, and some stage-1 patches enter stage-2. $\pi_{x,t}$ patches of stage-x enter the wet season. For the first stage,
86 $\pi_{1,\ t} = \xi_1(1-q_{12})P_{1,t}$, and for the second stage, $\pi_{2,\ t} = \xi_1 q_{12} P_{1,t} + \xi_2 P_{2,t}$. ξ_x is the fraction of stage-x patches persisting through the dry season, and q_{12} is the fraction of surviving
88 stage-1 patches that transition to stage-2. The likelihood that a stage-x patch persists (ξ_x) depends on exogenous abiotic factors, not on spore density within a patch. But transition of
90 a patch to stage-2 represents a reduction in the concentration of free-living infectious propagules within the patch.

92 2.2 Infection dynamics

If a susceptible host acquires an infection during the wet season, it either recovers with
94 resistance or dies. Resistant hosts that avoid infection lose their partial immunity [Cizauskas et al. 2014a]. Completing the annual cycle, S_{t+1} is the number of hosts that
96 avoid infection during the wet season:

$$\begin{aligned} S_{t+1} &= e^{-(\beta_1\pi_{1,\ t}+\beta_2\pi_{2,\ t})}(\sigma_t + \rho_t) \\ &= e^{-(\beta_1\pi_{1,\ t}+\beta_2\pi_{2,\ t})}\left(\left[S_t + R_t\right]\left[g + \lambda e^{-\mu(S_t+R_t)}\right]\right) \end{aligned} \tag{2}$$

We treat encounters with stage-x infectious patches as independent Poisson processes.
98 $\beta_x \pi_{x,\,t}$ is the rate at which any host, susceptible or resistant, experiences infectious contact at a stage-x pathogen patch ($x = 1, 2$). During any wet season, an individual host makes at
100 most a single infectious contact, and then either dies or develops transient immunity. That is, 'exposure' without a chance of lethal infection is irrelevant to the dynamics.

102 We refer to the β_x as infectiousness rates, and take $\beta_1 \geq \beta_2$ for two reasons. The pathogen is an obligate killer, and carcasses of mortally infected hosts generate first-stage
104 patches. Nutrients from dead hosts increase plant productivity at the carcass site [Turner et al. 2014]. Hence we assume that the attractiveness of forage quality increases the
106 rate at which individual hosts are attracted to stage-1 patches. Secondly, the relative recency of stage-1 patches implies that infectious-spore densities will be greater in these
108 patches [Turner et al. 2016]. Consequently, we reasonably assume that the likelihood of infection, given encounter, will be greater in the more recent patches. The β_x values
110 combine attraction to patches and the chance of infection of hosts within patches.

When infection occurs, we take its virulence as the probability that the infected host dies.
112 Virulence depends on both the host and patch stage, and we use these probabilities to complete the annual cycle for resistant hosts:

$$R_{t+1} = \left[1 - e^{-(\beta_1 \pi_{1,t} + \beta_2 \pi_{2,t})}\right] \{\sigma_t \left([1 - \nu_{\sigma,1}]\theta_t + [1 - \nu_{\sigma,2}][1 - \theta_t]\right) + \rho_t \left([1 - \nu_{\rho,1}]\theta_t + [1 - \nu_{\rho,2}][1 - \theta_t]\right)\}$$

114 $\nu_{\sigma,x}$ is virulence when susceptible hosts incur stage-x infections; $\nu_{\rho,x}$ is virulence among resistant hosts infected at a stage-x patch. By the definition of resistance, $\nu_{\rho,x} < \nu_{\sigma,x}$. That
116 is, resistant hosts are less likely than susceptibles to succumb to infection. Any infection that does not lead to mortality leaves the host with temporary resistance

[Bagamian et al. 2013].

Outcomes of infectious exposure must be weighted by the encounter rates with the different patch stages: $\theta_t = \beta_1 \pi_{1,\,t} / \left(\beta_1 \pi_{1,\,t} + \beta_2 \pi_{2,\,t}\right)$. Substituting for wet-season densities and simplifying yields the annual dynamics $R_{t+1}(S_t, R_t, \theta_t)$:

$$\begin{aligned} R_{t+1} &= \left[1 - e^{-(\beta_1 \pi_{1,t} + \beta_2 \pi_{2,t})}\right] \\ &\quad \left\{\left[g(S_t + \gamma R_t) + \lambda(S_t + R_t) e^{-\mu(S_t + R_t)}\right] (\mathbf{Z}_\sigma \cdot \mathbf{H_t}) + g(1-\gamma) R_t (\mathbf{Z}_\rho \cdot \mathbf{H_t})\right\} \end{aligned} \quad (3)$$

where $(\mathbf{Z_i} \cdot \mathbf{H_t})$ is a scalar product. Virulence of stage-1 patches is greater: $\nu_{i,1} > \nu_{i,2}$ for $i = \sigma, \rho$. Greater density of the pathogen within stage-1 patches increases the chance that an infection acquired there proves lethal.

The number of stage-1 patches sums stage-1 patches that persisted through the last dry season without transition, plus new patches generated at carcass sites during the wet season:

$$P_{1,t+1} = \pi_{1,\,t} + \left[1 - e^{-(\beta_1 \pi_{1,t} + \beta_2 \pi_{2,t})}\right] \left\{\sigma_t [\nu_{\sigma,1} \theta_t + \nu_{\sigma,2}(1 - \theta_t)] + \rho_t [\nu_{\rho,1} \theta_t + \nu_{\rho,2}(1 - \theta_t)]\right\}$$

Substituting for wet-season counts gives the annual dynamics $P_{1,t+1}(S_t, R_t, \theta_t)$:

$$\begin{aligned} P_{1,t+1} &= \xi_1 (1 - q_{12}) P_{1,t} + \left[1 - e^{-(\beta_1 \pi_{1,t} + \beta_2 \pi_{2,t})}\right] \\ &\quad \left\{\left[g(S_t + \gamma R_t) + \lambda(S_t + R_t) e^{-\mu(S_t + R_t)}\right] (\mathbf{V}_\sigma \cdot \mathbf{H_t}) + g(1-\gamma) R_t (\mathbf{V}_\rho \cdot \mathbf{H_t})\right\} \end{aligned} \quad (4)$$

Environmental transmission occurs only at infectious patches, and not through direct contact with carcasses [Friedman and Yakubu 2013]. The number of stage-2 patches at time $(t+1)$ sums transitions from persisting stage-1 patches plus stage-2 patches that survived the last dry season:

$$P_{2,t+1} = \pi_{2,t} = \xi_1 \; q_{12} \; P_{1,t} + \xi_2 \; P_{2,t} \quad (5)$$

2.2.1 Model summary

Intraspecific competition and disease mortality regulate host population growth. Their relative strengths should govern population sizes and, more generally, the system's dynamic complexity. The annual cycle assumes that host self-regulation acts before mortality from infection. Hence, the 'Ricker term,' $e^{-\mu(S_t+R_t)}$, appears in the dynamics of both host classes, and in the dynamics of $P_{1,t}$. Essentially, intraspecific competition limits the number of hosts available to the pathogen, and so diminishes the potentially destabilizing effects of disease [May et al. 1981, Cavalieri and Kocak 1999].

2.3 The interaction matrix

The interaction matrix arrays the partial derivatives for each state variable's level at time $(t+1)$ as a function of each variable's level at time t [Neubert and Kot 1992]. The interaction matrix, the Jacobian, $\mathbf{M}$ has elements m_{rc}; $r, c = 1, 2, 3, 4$. Appendix B lists the m_{rc}. Standard methods use the eigenvalues of $\mathbf{M}$ to assess local stability of equilibria.

3 Disease-free dynamics and pathogen invasion

In the absence of disease, density-dependent natality regulates host numbers. If natality exceeds dry-season mortality, host extinction is unstable, and the positive equilibrium node is $S^* = [ln(\lambda) - ln(1-g)]/\mu$. S^* will be locally stable if:

$$0 < ln(\lambda) - ln(1-g) < 2/(1-g) \tag{6}$$

Greater dry-season survival can stabilize S^* by relaxing overcompensation. Increased natality, of course, can be destabilizing. For sufficiently large (λ/μ) the model should belong

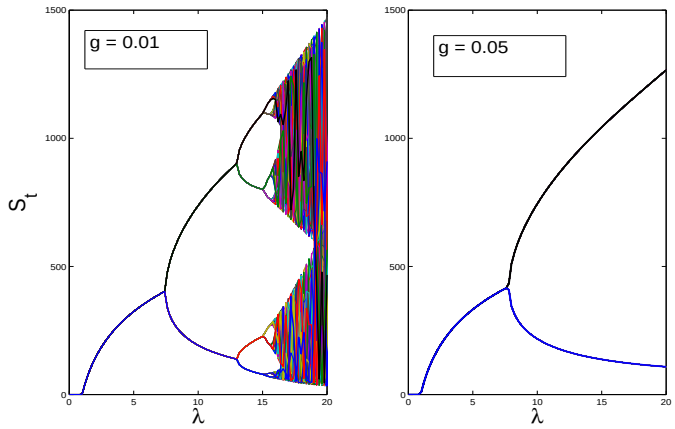

Figure 1: Dry-season survival and chaos. Bifurcation plots; $\mu = 0.005$ in each. Each plot shows susceptible population sizes for times $t = 251$ through $t = 2000$. Left plot: $g = 0.01$; period-doubling bifurcations, with increasing λ, take the dynamics to the chaotic regime. Right plot: $g = 0.05$; increased survival delays bifucations, and only a stable node and stable 2-cycle observed for $\lambda \leq 20$.

to the class of one-dimensional maps exhibiting the period-doubling route to chaos [Kaplan and Glass 1995]. Figure 1 shows bifurcation plots for two levels of dry-season survival g. For the lesser level of g, we see the bifurcation cascade. After increasing g, the dynamics bifurcates only once over the same range of λ. Given natality λ, increasing dry-season survival first delays, and then can eliminate, complex dynamics [Ruxton and Rohani 1998, Kaitala et al. 1999, Trainor and Caraco 2006]. See Appendix A.

3.1 Advance of the pathogen when rare

We introduce the pathogen into a disease-free host population as a single carcass, which becomes a stage-1 patch next wet season. The patch remains in the first stage for τ_1 wet seasons; τ_1 has a geometric probability distribution with mean $\langle \tau_1 \rangle = [1 - \xi_1(1 - q_{12})]^{-1}$. The initial stage-1 patch either decays or transitions to the second stage; the probability that the patch ever reaches stage-2 is $\xi_1 q_{12}/(\xi_1 q_{12} + 1 - \xi_1)$. Given transition to stage-2, the patch persists for τ_2 wet seasons. τ_2 has a geometric distribution with expectation

$\langle \tau_2 \rangle = (1 - \xi_2)^{-1}$.

For simplicity, we assume a stable disease-free host population with size S^*. The wet season host population has size $\sigma^* = S^*(g + \lambda e^{-\mu S^*}) = S^*$, in the absence of disease. When the pathogen is rare, the number of infectious patches generated over the expected lifetime of an initial patch is:

$$\Re_0 = S^* \left\{ \frac{(1 - e^{-\beta_1})\nu_{\sigma,1}}{[1 - \xi_1(1 - q_{12})]} + \frac{\xi_1 q_{12}}{\xi_1 q_{12} + 1 - \xi_1} \frac{(1 - e^{-\beta_2})\nu_{\sigma,2}}{(1 - \xi_2)} \right\} \tag{7}$$

$\Re_0$ is an expectation; we assume that the pathogen advances when rare if $\Re_0 > 1$. Since the pathogen is an obligate-killer, greater virulence always increases $\Re_0$, in the absence of functional dependence between pathogen traits [Day 2002, Caraco et al. 2014].

4 Fixed-point equilibria

This section restricts attention to fixed-point equilibria with the host extant. Suppose we hold all parameters but the rates of infectious exposure β_x constant. If β_1 and β_2, are sufficiently small, $\Re_0 < 1$, and the host population remains disease-free. The dry-season equilibrium node has $S^* > 0$, and $R^* = P_1^* = P_2^* = 0$.

Increasing infectious-exposure rates permits pathogen invasion, so that patch numbers P_x have positive equilibrium densities. When $[S^* R^* P_1^* P_2^*] > 0$, we have an interior equilibrium.

Given pathogen invasion, one boundary equilibrium can occur where all infections are mortal. If $\nu_{\sigma,1} = \nu_{\sigma,2} = 1$, then no infected host survives disease and $R^* = 0$. When dry-season survival is sufficiently smaller than the annual number of offspring per host at equilibrium ($g < \lambda \; exp\; \{-\mu S^*\}$), we can approximate this equilibrium node. Since $g < 1$ by definition, and host reproduction must compensate for disease mortality, the approximation should be reasonable. At the "maximal virulence" equilibrium infections are not too

common, but always lethal:

$$
\begin{aligned}
S^* &\approx \frac{ln[\lambda] - (\beta_1\pi_1^* + \beta_2\pi_2^*)}{\mu} && (8)\\
R^* &= 0 && (9)\\
P_1^* &\approx \frac{e^{(\beta_1\pi_1^* + \beta_2\pi_2^*)} - 1}{1 - \xi_1(1 - q_{12})} \; \frac{ln[\lambda] - (\beta_1\pi_1^* + \beta_2\pi_2^*)}{\mu} && (10)\\
P_2^* &= P_1^* \frac{\xi_1 \; q_{12}}{1 - \xi_2} && (11)
\end{aligned}
$$

The preceding is not a closed-form solution. But using $\beta_1\pi_1^* + \beta_2\pi_2^* = \xi_1 P_1^*[\beta_1(1 - q_{12})(1 - \xi_2) + \beta_2 q_{12}]$ allows numerical evaluation of P_1^*, and then S^* follows. Since we focus on pathogen population structure, we assume that $1 > \nu_{\sigma,1} \geq \nu_{\sigma,2}$ for the rest of the paper, and ignore the case where all infections are mortal.

As infectiousness continues to increase, $S^* \to 0$. In the limit, the host population, at the beginning of the dry season, includes only resistant individuals. Equivalently, neither newborns nor surviving resistant hosts escape contact with the pathogen during the wet season. At this limit we have the "maximal-exposure" boundary equilibrium:

$$
\begin{aligned}
S^* &= 0 && (12)\\
R^* &= \frac{ln[\lambda(\mathbf{Z}_\sigma \cdot \mathbf{H}^*)] - ln[1 - g(\gamma(\mathbf{Z}_\sigma \cdot \mathbf{H}^*) + (1 - \gamma)(\mathbf{Z}_\rho \cdot \mathbf{H}^*))]}{\mu} && (13)\\
P_1^* &= R^* \; \frac{(g\gamma + \lambda e^{-\mu R^*})(\mathbf{V}_\sigma \cdot \mathbf{H}^*) + g(1 - \gamma)(\mathbf{V}_\rho \cdot \mathbf{H}^*)}{1 - \xi_1(1 - q_{12})} && (14)\\
P_2^* &= P_1^* \frac{\xi_1 \; q_{12}}{1 - \xi_2} && (15)
\end{aligned}
$$

If π_1^* and π_2^* are the equilibrium patch numbers during the wet season, we have at equilibrium $\theta_1^* = \beta_1\pi_1^*/(\beta_1\pi_1^* + \beta_2\pi_2^*)$. The maximal-exposure equilibrium depends on θ_1^*,

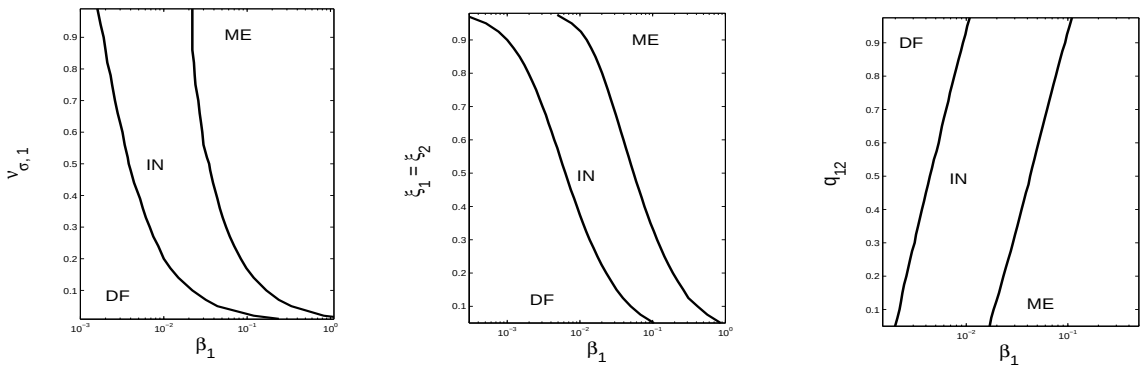

Figure 2: Point equilibria: disease-free (DF), interior (IN), and maximal exposure (ME). All plots: $\lambda = 3$, $g = 0.6$, $\mu = 0.005$, $\gamma = 0.7$, and $\beta_2 = \beta_1/2$; $\nu_{\sigma,2} = \nu_{\sigma,1}/3$, $\nu_{\rho,1} = \nu_{\sigma,1}/2$, and $\nu_{\rho,2} = \nu_{\sigma,1}/6$. Left plot: $\xi_1 = \xi_2 = 0.7$, $q_{12} = 0.3$. Center plot: $q_{12} = 0.3$. $\nu_{\sigma,1} = 0.6$. Right plot: $\xi_1 = \xi_2 = 0.7$, $\nu_{\sigma,1} = 0.6$. Equilibria locally stable (numerical checks).

which simplifies to:

$$\theta_1^* = \beta_1(1 - q_{12}) / \left(\beta_1(1 - q_{12}) + \beta_2 \left[\frac{q_{12}}{1 - \xi_2} \right] \right) \tag{16}$$

Then the vector $\mathbf{H}^* = [\theta_1^*,\ 1 - \theta_1^*]$. Intuitively, θ_1^* increases with β_1, and decreases with both β_2 and ξ_2. Computationally, we report the maximal-exposure equilibrium when $S^* < 1$.

Figure 2 shows non-overlapping regions of the model's stable point equilibria. In each plot, as infectiousness levels β_x increase, the disease-free equilibrium gives way to the interior equilibrium, which in turn yields to the maximal-exposure equilibrium. Increasing either the virulence of infections (left plot) or the survival of pathogen patches (center plot) decreases both the minimal infectiousness required for pathogen invasion and the levels of infectiousness necessary for maximal exposure. However, increasing q_{12}, the stage-1 to stage-2 transition probability, has the opposite effects. A larger q_{12} reduces the mean infectiousness and mean virulence across all pathogen patches, and so hinders the pathogen's invasion of a disease-free host population.

5 Structured infectiousness

Understanding the ecological significance of pathogen-patch structure requires comparison of disease dynamics in the presence and absence of structure. Appendix C presents the reduced version of our model where all patches are ecologically and epidemiologically identical.

This section and the following two sections address, in order, structure in infectiousness, virulence, and patch persistence. In each case we emphasize effects on internal-equilibrium population sizes at different levels of the stage transition probability q_{12}, the probability that a stage-1 patch transitions to the second stage.

To analyze patch-structured infectious-exposure rates β_x, we take infectiousness structure as increasing with the between-stage difference $\beta_1 - \beta_2 \geq 0$. Let $\beta_1 = \beta_0 + \delta_\beta$, and $\beta_2 = \beta_0 - \delta_\beta$; increasing δ_β increases pathogen structure.

5.1 Structured infectiousness and natality

Figure 3 offers a baseline example for structured infectiousness. Once natality λ exceeds a critical value, the pathogen invades and the interior equilibrium is stable over the remaining range of λ plotted. Infectious patches and resistant host numbers increase with λ, while susceptible hosts start to decline at pathogen invasion. The increase in infectious-patch number with natality does not reduce total host-population size, since growth of resistance keeps pace with loss of susceptible individuals.

For any stable internal equilibrium, Figure 3 shows that increased infectiousness structure reduces the number of susceptibles. Simultaneously, resistant hosts and both patch stages become more abundant. Increased pathogen structure advances pathogen growth by killing more hosts. At the same time, the host population averts decline because more hosts acquire temporary resistance and reduce the average mortality among hosts encountering

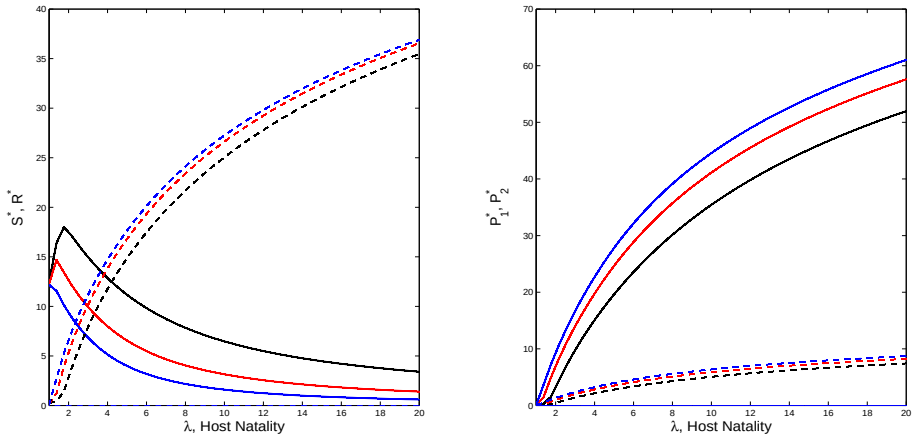

Figure 3: Patch encounters and population sizes: interior equilibria. Left plot: Solid lines are susceptible hosts; dashed lines are resistant hosts. Right plot: Solid lines are number of stage-1 patches; dashed lines show numbers of stage-2 patches. Both plots: Black shows results for $\beta_1 = 0.11$ and $\beta_2 = 0.09$; red shows results for $\beta_1 = 0.14$ and $\beta_2 = 0.06$; blue shows results for $\beta_1 = 0.17$ and $\beta_2 = 0.03$ Other parameters: $g = 0.6$, $\gamma = 0.4$, $\mu = 0.1$; $\nu_{\sigma,1} = 0.6$, $\nu_{\rho,1} = 0.3$, $\nu_{\sigma,2} = 0.4$, $\nu_{\rho,2} = 0.1$, $\xi_1 = \xi_2 = 0.4$, and $q_{12} = 0.25$.

infectious patches the next year.

The strength of self-regulation in the host dynamics should affect the equilibrium disease ecology. To demonstrate, we made a single change in baseline parameters, reducing μ from 0.1 to 0.01. This relaxes the host's intraspecific regulation of natality, leaving the host population subject to stronger density-dependent regulation through virulent infection. Figure 4 shows the consequences. At low levels of λ, $S^* \to 0$ (S^* falls below unity), and only resistant hosts remain. Reducing the relative strength of host self-regulation leads to large increases in the numbers of both infectious-patch stages. Interestingly, the increase in patch numbers is accompanied by an increase in the total number of hosts, although the dry season begins with only resistant individuals: the maximal-exposure equilibrium. Stronger interspecific regulation of host growth increases equilibrium host density after the shift in equilibria.

As noted above, reducing the buffering effect of the host's dry-season survival can

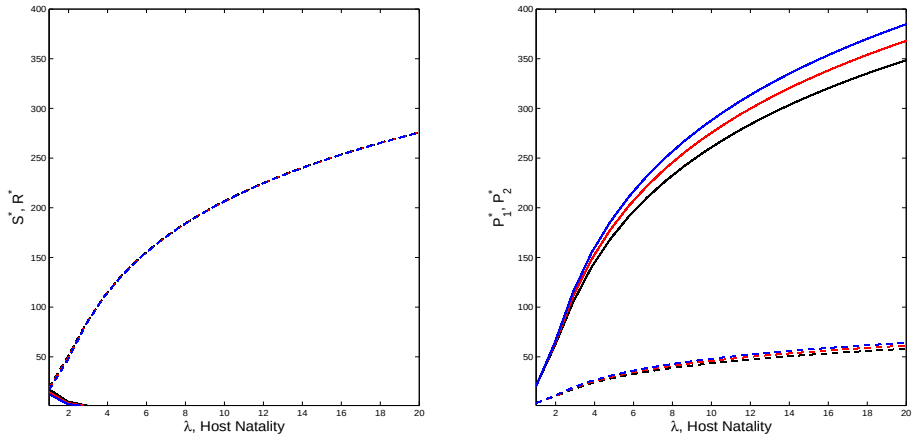

Figure 4: Patch encounters and population sizes: maximal-exposure equilibria. Line density, colors same as Fig. 3. Parameter values, with one exception, exactly as in Fig. 3. Single change: μ reduced to 0.01, to relax strength of density-dependent limitation on host natality. Note logarithmic scaling of the left plot's ordinate. Increasing regulation of host by pathogen results in larger number of hosts, but frequency of resistance quickly approaches unity, and susceptible hosts are not found during the dry season.

generate cycling in the equilibrium disease ecology. To demonstrate, we changed in baseline parameter by reducing g from 0.6 to 0.06. Figure 10 shows the anticipated consequence. The dynamics transitions from a stationary node to a stable 2-cycle as λ increases. Over the course of a single cycle, greater infectiousness structure produces more infectious patches, fewer susceptible hosts, and more resistant hosts.

6 Structured virulence

We let virulence structure increase with the difference $(\nu_{\sigma,1} - \nu_{\sigma,2})$. We set $\nu_{\sigma,1} = \nu_0 + \delta_\nu$, and $\nu_{\sigma,2} = \nu_0 - \delta_\nu$. As a convenience, we maintain $\nu_{\rho,x} = \nu_{\sigma,x}/k$, where $k > 1$. Increasing δ_ν, increasing virulence structure, increases lethal-infection frequency in stage-1 patches, and decreases the frequency in stage-2 patches. Here we examine interaction between virulence structure and q_{12}, the probability of transition from a first-stage to second-stage infectious

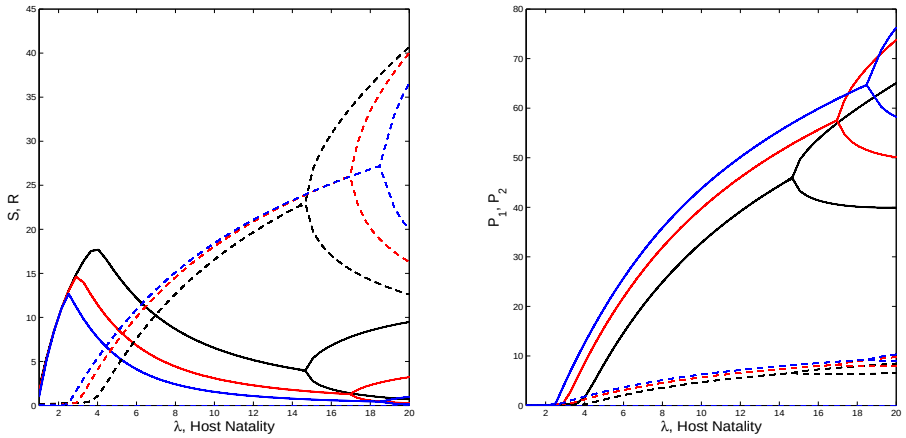

Figure 5: Patch encounters and population sizes: host survival and cycles. Parameter values, with one exception, exactly as in Fig. 3. Single change: dry-season survival reduced to $g = 0.06$. β values, both plots: red shows results for $\beta_1 = 0.14$ and $\beta_2 = 0.06$; red shows results for $\beta_1 = 0.17$ and $\beta_2 = 0.03$. Reduced dry-season survival allows (first) period-doubling bifurcation.

patch.

Figure 6 shows that any increase in the rate of transition from first to a second-stage patch increases total host numbers, while the frequency of resistance among hosts and the number of infectious patches both decline. Increasing q_{12} decreases the abundance of first-stage, and increases abundance of second-stage, patches. Since the latter produce fewer exposures per patch ($\beta_2 < \beta_1$) and are less virulent, given exposure ($\nu_{i,2} \leq \nu_{i,1}$), the effects of q_{12} make intuitive sense.

The effects of increasing virulence structure depend on the value of q_{12}. When stage-1 patches are relatively long lasting ($q_{12} < 1/2$) total host number decreases as δ_ν increases, while the frequency of resistance and infectious-patch counts correspondingly increase. However, when $q_{12} > 1/2$, total host number increases with virulence structure, and both resistance frequency and the number of stage-1 patches decline as δ_ν increases. When q_{12} becomes sufficiently large, most patches will be in the second stage. Given that increased structure renders second-stage patches less virulent, total host number can increase, and P_1

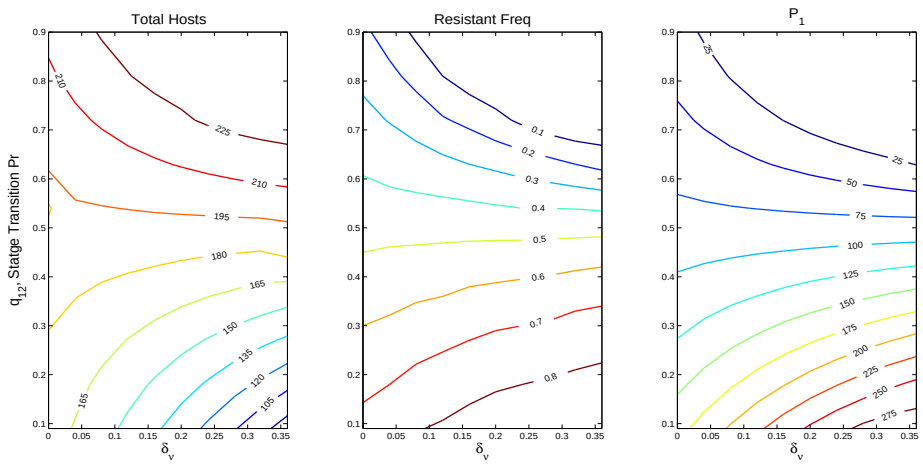

Figure 6: Virulence structure and stage transition probability. Left plot contours: $(S^* + R^*)$; center plot contours: $R^*/(S^* + R^*)$; right plot contours: P_1. Parameters as in Fig. 14, with $\gamma = 0.6$.

declines concurrently. Since second-stage patches generate exposure to the pathogen at a lesser rate, the frequency of resistance can decline. Different stage structures for pathogen patches can strongly affect host numbers and the fraction of hosts exhibiting resistance.

6.1 Comparison to unstructured model

When pathogen patches lack structure, $q_{12} = 0$ and $\delta_\nu = 0$; again, $\beta_0 = 0.015$. If the structured pathogen's stage-transition probability q_{12} is relatively small, which increases the duration of stage-1 patches, then host numbers are larger, stage-1 patch numbers are smaller, and fewer hosts proportionally exhibit resistance in the absence of virulence structure. However, when q_{12} is relatively large, host numbers are smaller, infectious patches are more numerous, and resistance frequency is greater in the absence of structure. The first result (low q_{12}) compares the unstructured model with a more infectious, more virulent pathogen-environment. Hence the host population is larger in the absence of pathogen structure. The second result (high q_{12}) compares the unstructured model with a less infectious, less virulent pathogen-environment. A larger q_{12} shifts the patch stage

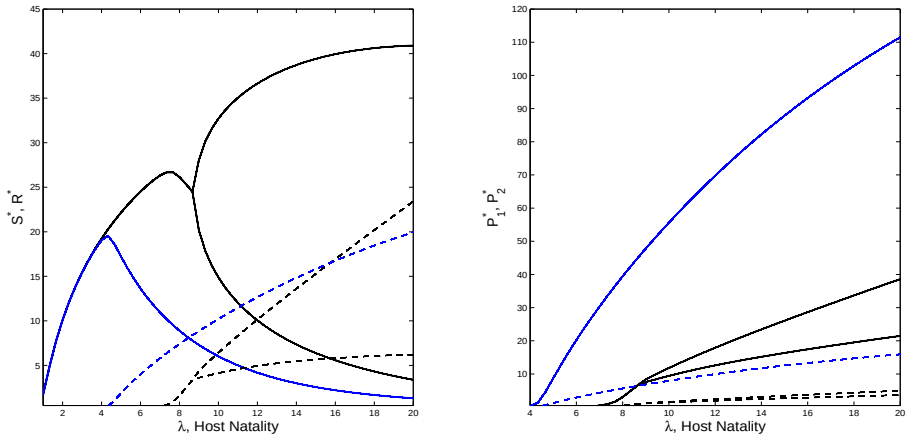

Figure 7: Virulence and population sizes: host survival and cycles. Parameter values, with one exception, exactly as in Fig. **??**. Single change: dry-season survival reduced to $g = 0.06$. Left plot: hosts, as in Fig. **??**; right plot: pathogen patches, as in Fig. **??**.

structure to a greater relative abundance of stage-2, hence less virulent, patches. Increased virulence structure (larger δ_ν) decreases the average virulence in the environment, and so host number increases as virulence structure increases.

6.2 Structured virulence and natality

In Figure srpvir1 the interior equilibrium is locally stable for, essentially, the entire range of λ plotted. Increased natality quickly leads to fewer susceptible, and more resistant, hosts entering the dry season. For fixed virulence levels, the total number of hosts increases along with the number of infectious patches as λ increases. Host and patch totals grow concurrently since the increase in R^* exceed the decrease in S^*.

At any λ where the pathogen can invade, greater virulence structure decreases the number of susceptible hosts at equilibrium. That is, susceptible number declines as δ_ν increases for fixed natality in Figure **??**. Greater δ_ν, of course, increases the number of both stage-1 and stage-2 patches.

Decreasing μ relaxes host-self-regulation, increasing the relative strength of regulation by

disease. Decreasing dry-season survival g should increase dynamic complexity; Figure 7 shows the results. The dynamics exhibits a period-doubling bifurcation; lower survival values produce greater dynamic complexity.

In the absence of patch structure, $\delta_\nu = 0$, and $\delta_\xi = 0$. The addition of pathogen structure, for these parameters, always reduces host number, while both infectious patches and resistance frequency increase.

6.3 Stage transition probabilities and patch structure

This section shows how varying the pathogen‘s stage transition probabilities induces pattern in the population dynamics. First, we increase the between-stage transition probability q_{12}. Then, separately, we increase the difference between stage-specific survival rates, $\delta_\xi = \xi_1 - \xi_2 \geq 0$.

In Figure srpq21a, increasing q_{12} affects both the absolute and relative abundances of the patch stages. The interior equilibrium remains locally stable over the entire range of λ for the baseline parameter values. Increasing q_{12} allows an increase in the number of susceptibles, and decreases the number of resistant hosts. Not surprisingly, the number of stage-1 patches declines as q_{12} increases. The interaction of faster transition from stage-1 to stage-2 and the simultaneous decline in stage-1 patches leaves the number of stage-2 patches a non-monotonic function of q_{12}, at baseline parameters.

Decreasing the strength of host self-regulation, relative to regulation by disease mortality, again shifts the system (effectively) to the maximal-exposure equilibrium. Susceptibles disappear during the wet season, and total host numbers increase *via* growth of the resistant category; see Figure srpq21b. Essentially, relaxing self-regulation releases host reproduction sufficient to fuel “vaccination” at stage-2 patches, and the host population increases in size. Again, reducing dry-season survival allows increased dynamic complexity

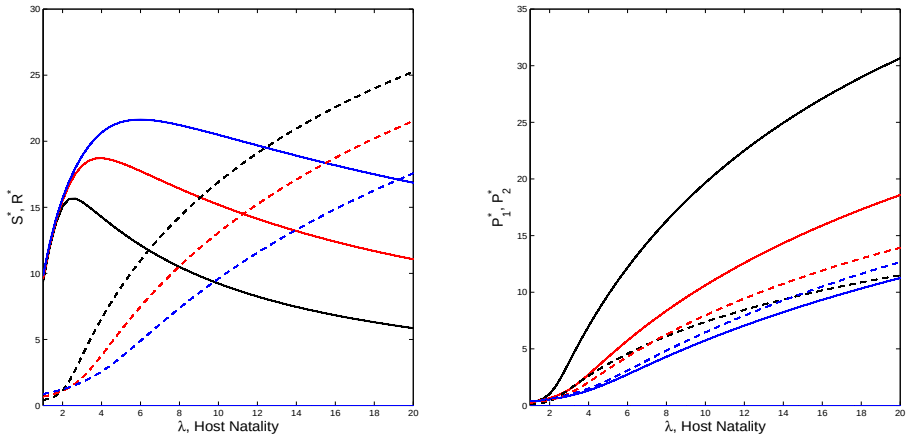

Figure 8: Stage transitions and population sizes: internal equilibria. Parameter values, with one exception, exactly as in Fig. 3. Single change: dry-season survival reduced to $g = 0.06$. β values, both plots: red shows results for $\beta_1 = 0.14$ and $\beta_2 = 0.06$; red shows results for $\beta_1 = 0.17$ and $\beta_2 = 0.03$. Reduced dry-season survival allows (first) period-doubling bifurcation.

(not shown). Once populations exhibit a 2-cycle, larger q_{12} increases cycle amplitude in susceptible hosts, and reduces amplitude of the resistant-host cycle. As the patch-survival difference δ_ξ increases, susceptible numbers decline, while both resistant-host and infectious-patch numbers increase. Figure srpdeltaxi shows baseline results. Reducing either the relative strength of host self-regulation or dry-season survival induces patterns qualitatively matching those reported above.

7 Interacting pathogen life-history traits

Suppose, for example, that greater investment in the free-living pathogen‘s exosporium increases patch persistence ξ_x. Increased spore size will increase survival, but might imply lower spore number, or might reduce initial within-host growth rate to a level where virulence declines.

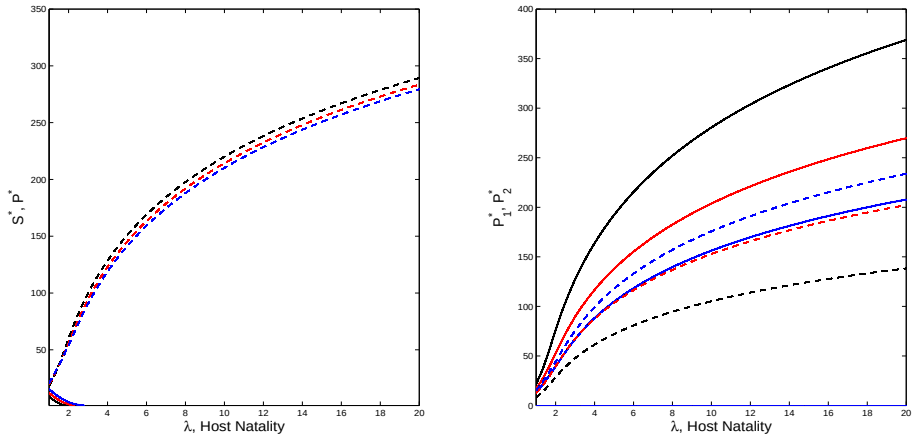

Figure 9: Stage transitions and population sizes: maximal-exposure equilibria. Parameter values, with one exception, exactly as in Fig. 3. Single change: dry-season survival reduced to $g = 0.06$. β values, both plots: red shows results for $\beta_1 = 0.14$ and $\beta_2 = 0.06$; red shows results for $\beta_1 = 0.17$ and $\beta_2 = 0.03$. Reduced dry-season survival allows (first) period-doubling bifurcation.

7.1 Virulence structure: Interaction with structured patch persistence

More recent patches should hold greater numbers of infectious particles. Depending on the abiotic factors faced during the dry season, the greater number of free-living particles might imply that more recent patches have greater annual persistence than the across-stage average. We refer to any increase in $(\xi_1 - \xi_2)$ as increased persistence structure.

We set $\xi_1 = 0.5 + \delta_\xi$, and $\xi_2 = 0.5 - \delta_\xi$. This section asks how host and pathogen-patch numbers vary as levels of δ_ν and δ_ξ increase. Figure 11 shows that increased virulence structure again reduces host number, increases resistance frequency, and increases infectious-patch number. Persistence structure has the same qualitative effects. The frequency of resistance responds strongly to δ_ν; as δ_ν increases, stage-1 patches become killers, and stage-2 patches become vaccinators.

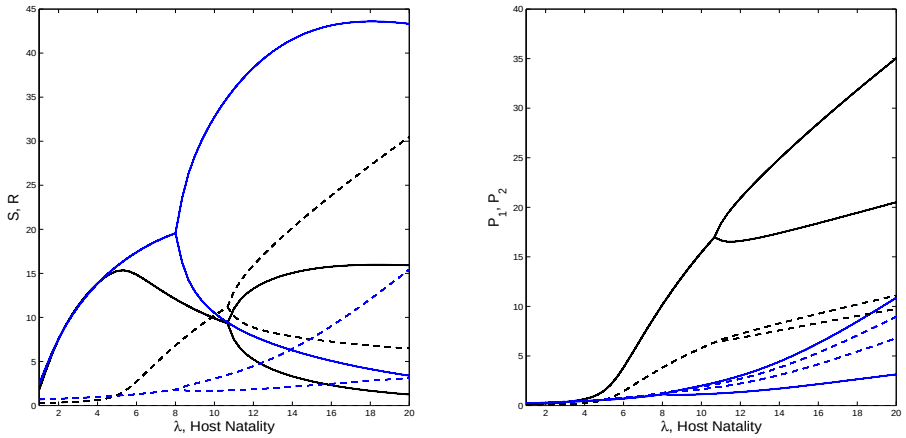

Figure 10: Patch encounters and population sizes: dry-season survival and cycles. Parameter values, with one exception, exactly as in Fig. 3. Single change: dry-season survival reduced to $g = 0.06$. β values, both plots: red shows results for $\beta_1 = 0.14$ and $\beta_2 = 0.06$; red shows results for $\beta_1 = 0.17$ and $\beta_2 = 0.03$. Reduced dry-season survival allows (first) period-doubling bifurcation.

8 Discussion

Spatial localization of an obligate-killing, free-living pathogen implies that age or stage structure of infectious patches should influence both the pattern of exposure to the pathogen, and the probability of lethal infection following exposure. Our model pathogen's impact on host-population regulation depends on its stage structure, the infectious-exposure rates, and virulence levels. The degree to which patch stages differ in their impact on host mortality will govern the complexity of the host-pathogen population dynamics, and impact the chance that pathogen strains differing in life-history traits can coexist.

The model does not distinguish low-dose exposure prompting a small (but detectable) sero-conversion and higher-dose infection resulting in recovery and transient immune resistance [Bagamian et al. 2013].

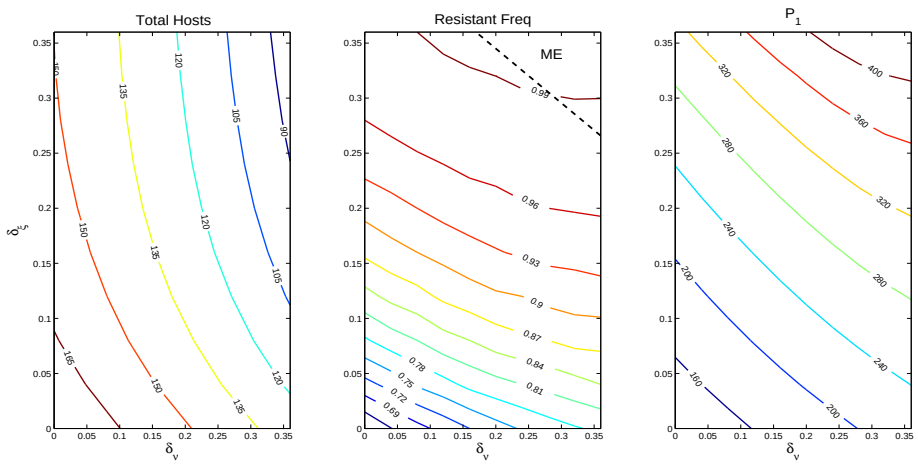

Figure 11: Virulence structure and patch-persistence structure. Left plot contours: (S^*+R^*); center plot contours: $R^*/(S^*+R^*)$; right plot contours: P_1. Parameters as in Fig. 14, with $q_{12} = 0.25$. In this example, susceptible number S^* goes effectively to zero; the maximal-exposure equilibrium is outlined on the plot of resistance frequency.

A Disease-free model

The disease-free dynamics reduces to a Ricker-like map [Avilés 1999]. Increasing host natality λ generates a cascade of period-doubling bifurcations. Given μ, which scales self-regulation of host reproduction, the locally stable equilibrium node $S^* > 0$ becomes unstable, and a period-2 cycle becomes stable, at the first pitchfork bifurcation; see Fig. 12. We let $\lambda_1(g)$ represent the natality, as a function of dry-season survival g, where the first bifurcation occurs. From the stability criterion for S^*, Equation (6), we have:

$$\lambda_1(g) = (1-g)exp\{2/(1-g)\} \tag{B.1}$$

$\lambda_1(g)$ increases convexly with g ($\lambda_1(g)$, and does not depend on μ. Given the nonbreeding season survival of most large herbivores, we would not anticipate annual natality per individual large enough to meet the model‘s criterion for complex (deterministic) disease-free dynamics.

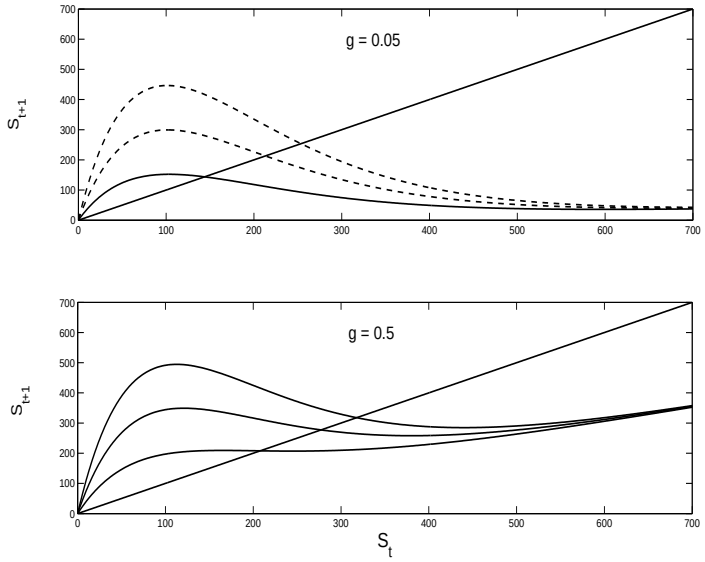

Figure 12: Disease-free host dynamics. At equilibrium, $S_{t+1} = S_t$. In each plot the positive equilibrium node S^* increases with host natality $\lambda = 4, 8, 12$. Upper plot: Low dry-season survival generates strong overcompensation. Broken 1-D maps (for $\lambda = 8$ and 12) indicate S^* unstable. Lower plot: Increased dry-season survival both increases and stabilizes positive equilibrium nodes for the same natality levels. $\mu = 0.01$ for each map.

B The interaction matrix M

The m_{rc} elements of the interaction matrix or Jacobian [Neubert and Kot 1992], follow.

$$m_{11} = \frac{\partial S_{t+1}}{\partial S_t} = e^{-(\beta_1 \pi_{1,t} + \beta_2 \pi_{2,t})} \left(g - \lambda e^{-\mu(S_t + R_t)} \left[\mu S_t - 1 \right] \right) \tag{A.1}$$

$$m_{12} = \frac{\partial S_{t+1}}{\partial R_t} = e^{-(\beta_1 \pi_{1,t} + \beta_2 \pi_{2,t})} \left(g - \lambda e^{-\mu(S_t + R_t)} \left[\mu R_t - 1 \right] \right) \tag{A.2}$$

The net impact of host numbers on growth of the susceptible population integrates dry-season survival and self-regulation.

$$\begin{aligned} m_{13} \;=\; \frac{\partial S_{t+1}}{\partial P_{1,t}} &= -e^{-(\beta_1 \pi_{1,t} + \beta_2 \pi_{2,t})} \left([S_t + R_t][g + \lambda e^{-\mu(S_t + R_t)}] \right) \\ &\quad (\xi_1 [\beta_1 (1 - q_{12}) + \beta_2 q_{12}]) < 0 \end{aligned} \tag{A.3}$$

$$m_{14} = \frac{\partial S_{t+1}}{\partial P_{2,t}} = -\beta_2 \xi_2 \; e^{-(\beta_1 \pi_{1,t} + \beta_2 \pi_{2,t})} \left([S_t + R_t][g + \lambda e^{-\mu(S_t + R_t)}] \right) < 0 \tag{A.4}$$

Increasing the number of either infectious-patch stage reduces growth of susceptible hosts.

$$m_{21} = \frac{\partial R_{t+1}}{\partial S_t} = [1 - e^{-(\beta_1 \pi_{1,t} + \beta_2 \pi_{2,t})}] \left(g - \lambda e^{-\mu(S_t + R_t)} \left[\mu S_t - 1 \right] \right) (\mathbf{Z}_\sigma \cdot \mathbf{H}_t) \tag{A.5}$$

$$m_{22} = \frac{\partial R_{t+1}}{\partial R_t} = [1 - e^{-(\beta_1 \pi_{1,t} + \beta_2 \pi_{2,t})}] \{ [g\lambda - \lambda e^{-\mu(S_t + R_t)} (\mu R_t - 1)] (\mathbf{Z}_\sigma \cdot \mathbf{H}_t) + g(1-\gamma)(\mathbf{Z}_\rho \cdot \mathbf{H}_t) \} \tag{A.6}$$

In expressions to follow, we shall use the following two partial derivatives:

$$\frac{\partial \theta_t}{\partial P_{1,t}} = \frac{\beta_1 \beta_2 \xi_1 \xi_2 (1 - q_{12}) P_{2,t}}{\left[\beta_1 \xi_1 (1 - q_{12}) P_{1,t} + \beta_2 \xi_1 q_{12} P_{1,t} + \beta_2 \xi_2 P_{2,t} \right]^2} \tag{A.7}$$

$$\frac{\partial \theta_t}{\partial P_{2,t}} = -\frac{P_{1,t}}{P_{2,t}} \frac{\partial \theta_t}{\partial P_{1,t}} \tag{A.8}$$

354 Proceeding with the elements of $\mathbf{M}$:

$$\begin{aligned} m_{23} \quad = \quad & \frac{\partial R_{t+1}}{\partial P_{1,t}} = \left[g(S_t + \gamma R_t) + \lambda (S_t + R_t) e^{-\mu(S_t + R_t)} \right] \frac{\partial \theta_t}{\partial P_{1,t}} \left[\nu_{\sigma,2} - \nu_{\sigma,1} \right] \\ + \quad & e^{-(\beta_1 \pi_{1,t} + \beta_2 \pi_{2,t})} [g(S_t + \gamma R_t) + \lambda (S_t + R_t) e^{-\mu(S_t + R_t)}] \\ & \left(\xi_1 [\beta_1 (1 - q_{12}) + \beta_2 q_{12}] (\mathbf{Z}_\sigma \cdot \mathbf{H}_t) + \frac{\partial \theta_t}{\partial P_{1,t}} \left[\nu_{\sigma,1} - \nu_{\sigma,2} \right] \right) \\ + \quad & [g(1-\gamma) R_t] \frac{\partial \theta_t}{\partial P_{1,t}} \left[\nu_{\rho,2} - \nu_{\rho,1} \right] \\ + \quad & e^{-(\beta_1 \pi_{1,t} + \beta_2 \pi_{2,t})} [g(1-\gamma) R_t] \left(\xi_1 [\beta_1 (1 - q_{12}) + \beta_2 q_{12}] (\mathbf{Z}_\rho \cdot \mathbf{H}_t) + \frac{\partial \theta_t}{\partial P_{1,t}} \left[\nu_{\rho,1} - \nu_{\rho,2} \right] \right) \end{aligned} \tag{A.9}$$

The first and third terms of the sum must be negative, and the second and fourth terms

must be positive.

$$
\begin{aligned}
m_{24} \quad &= \quad \frac{\partial R_{t+1}}{\partial P_{2,t}} = \left[g(S_t + \gamma R_t) + \lambda(S_t + R_t)e^{-\mu(S_t+R_t)}\right] \frac{\partial \theta_t}{\partial P_{2,t}} \left[\nu_{\sigma,2} - \nu_{\sigma,1}\right] \\
&+ \quad e^{-(\beta_1 \pi_{1,t} + \beta_2 \pi_{2,t})}[g(S_t + \gamma R_t) + \lambda(S_t + R_t)e^{-\mu(S_t+R_t)}] \\
&\quad \left(\beta_2 \xi_2(\mathbf{Z}_\sigma \cdot \mathbf{H}_t) + \frac{\partial \theta_t}{\partial P_{2,t}} \left[\nu_{\sigma,1} - \nu_{\sigma,2}\right]\right) \\
&+ \quad [g(1-\gamma)R_t]\frac{\partial \theta_t}{\partial P_{2,t}} \left[\nu_{\rho,2} - \nu_{\rho,1}\right] \\
&+ \quad e^{-(\beta_1 \pi_{1,t} + \beta_2 \pi_{2,t})}[g(1-\gamma)R_t] \left(\beta_2 \xi_2(\mathbf{Z}_\rho \cdot \mathbf{H}_t) + \frac{\partial \theta_t}{\partial P_{2,t}} \left[\nu_{\rho,1} - \nu_{\rho,2}\right]\right)
\end{aligned}
\tag{A.10}
$$

In this case, the first and third terms are positive; signs of the second and fourth terms depend on where the partial is evaluated. Hence, under some conditions, the growth of the number of resistant hosts will increase as the number of stage-2 patches increases, a natural 'vaccinator' effect.

Proceeding,

$$
m_{31} = \frac{\partial P_{1,t+1}}{\partial S_t} = [1 - e^{-(\beta_1 \pi_{1,t} + \beta_2 \pi_{2,t})}](\mathbf{V}_\sigma \cdot \mathbf{H}_t) \left(g - \lambda e^{-\mu(S_t+R_t)} \left[\mu S_t - 1\right]\right) \tag{A.11}
$$

$$
m_{32} = \frac{\partial P_{1,t+1}}{\partial R_t} = [1 - e^{-(\beta_1 \pi_{1,t} + \beta_2 \pi_{2,t})}]\{(\mathbf{V}_\sigma \cdot \mathbf{H}_t) \left(g - \lambda e^{-\mu(S_t+R_t)} \left[\mu R_t - 1\right]\right) + g(1-\gamma)(\mathbf{V}_\rho \cdot \mathbf{H}_t)\} \tag{A.12}
$$

$$
\begin{aligned}
m_{33} \quad &= \quad \frac{\partial P_{1,t+1}}{\partial P_{1,t}} = \xi_1(1-q_{12}) + \left[g(S_t+\gamma R_t) + \lambda(S_t+R_t)e^{-\mu(S_t+R_t)}\right] \frac{\partial \theta_t}{\partial P_{1,t}} \left[\nu_{\sigma,1} - \nu_{\sigma,2}\right] \\
&+ \quad e^{-(\beta_1\pi_{1,t}+\beta_2\pi_{2,t})} \left[g(S_t+\gamma R_t) + \lambda(S_t+R_t)e^{-\mu(S_t+R_t)}\right] \\
&\quad \left(\xi_1[\beta_1(1-q_{12}) + \beta_2 q_{12}](\mathbf{V}_\sigma \cdot \mathbf{H}_t) + \frac{\partial \theta_t}{\partial P_{1,t}} \left[\nu_{\sigma,2} - \nu_{\sigma,1}\right]\right) \\
&+ \quad [g(1-\gamma)R_t] \frac{\partial \theta_t}{\partial P_{1,t}} \left[\nu_{\rho,1} - \nu_{\rho,2}\right] \qquad \text{(A.13)} \\
&+ \quad e^{-(\beta_1\pi_{1,t}+\beta_2\pi_{2,t})}[g(1-\gamma)R_t]\{\xi_1[\beta_1(1-q_{12}) + \beta_2 q_{12}](\mathbf{V}_\rho \cdot \mathbf{H}_t) + \frac{\partial \theta_t}{\partial P_{1,t}} \left[\nu_{\rho,2} - \nu_{\rho,1}\right]\}
\end{aligned}
$$

$$
\begin{aligned}
m_{34} \quad &= \quad \frac{\partial P_{1,t+1}}{\partial P_{2,t}} = \left[g(S_t+\gamma R_t) + \lambda(S_t+R_t)e^{-\mu(S_t+R_t)}\right] \frac{\partial \theta_t}{\partial P_{2,t}} \left[\nu_{\sigma,1} - \nu_{\sigma,2}\right] \\
&+ \quad e^{-(\beta_1\pi_{1,t}+\beta_2\pi_{2,t})} \left[g(S_t+\gamma R_t) + \lambda(S_t+R_t)e^{-\mu(S_t+R_t)}\right] \\
&\quad \left(\beta_2\xi_2(\mathbf{V}_\sigma \cdot \mathbf{H}_t) + \frac{\partial \theta_t}{\partial P_{2,t}} \left[\nu_{\sigma,2} - \nu_{\sigma,1}\right]\right) \\
&+ \quad [g(1-\gamma)R_t] \frac{\partial \theta_t}{\partial P_{2,t}} \left[\nu_{\rho,1} - \nu_{\rho,2}\right] \qquad \text{(A.14)} \\
&+ \quad e^{-(\beta_1\pi_{1,t}+\beta_2\pi_{2,t})}[g(1-\gamma)R_t] \left(\beta_2\xi_2(\mathbf{V}_\rho \cdot \mathbf{H}_t) + \frac{\partial \theta_t}{\partial P_{2,t}} \left[\nu_{\rho,2} - \nu_{\rho,1}\right]\right)
\end{aligned}
$$

$$
m_{41} = \frac{\partial P_{2,t+1}}{\partial S_t} = 0 = \frac{\partial P_{2,t+1}}{\partial R_t} = m_{42} \qquad \text{(A.15)}
$$

$$
m_{43} = \frac{\partial P_{2,t+1}}{\partial P_{1,t}} = \xi_1 q_{12} > 0 \qquad \text{(A.16)}
$$

Finally,

$$
m_{44} = \frac{\partial P_{2,t+1}}{\partial P_{2,t}} = \xi_2 > 0 \qquad \text{(A.17)}
$$

C Infectious patches without structure

362 The unstructured dynamics assumes identical infectious patches. Then:

$$S_{t+1} = e^{-\beta_0 \pi_{0,t}} \left([S_t + R_t] \left[g + \lambda e^{-\mu(S_t+R_t)} \right] \right) \tag{C.1}$$

$$R_{t+1} = \left[1 - e^{-\beta_0 \pi_{0,t}}\right] \left\{ \left[g(S_t + \gamma R_T) + \lambda (S_t + R_t) e^{-\mu(S_t+R_t)} \right] [1 - \nu_{\sigma,0}] + g(1-\gamma) R_t [1 - \nu_{\rho,0}] \right\} \tag{C.2}$$

$$P_{0,t+1} = \xi_0 P_{0,t} + \left[1 - e^{-\beta_0 \pi_{0,t}}\right] \left\{ \left[g(S_t + \gamma R_T) + \lambda (S_t + R_t) e^{-\mu(S_t+R_t)} \right] \nu_{\sigma,0} + g(1-\gamma) R_t \nu_{\rho,0} \right\} \tag{C.3}$$

The subscript 0 refers to values for the unstructured dynamics. $P_{0,t}$ is the number of identical pathogen patches in the dry season. π_0 counts patches during the wet season; $\pi_0 = \xi_0 P_{0,t}$. For meaningful comparison, we set $\beta_0 = \beta_1 + \beta_2$, fixing infectious exposure events per host, per patch, between the structured and unstructured cases. In parallel, $\nu_{\sigma,0}$ ($\nu_{\rho,0}$) is the arithmetic mean of the structured $\nu_{\sigma,x}$ ($\nu_{\rho,x}$). We also equate a patch's mean "lifetime" for the two cases, so that:

$$(1 - \xi_0)^{-1} = \langle \tau_1 \rangle + \frac{\xi_1 q_{12}}{1 - \xi_1 + \xi_1 q_{12}} \langle \tau_2 \rangle = \frac{1}{1 - \xi_1 + \xi_1 q_{12}} \left[1 + \frac{\xi_1 q_{12}}{1 - \xi_2} \right] \tag{C.4}$$

In the pathogen's absence, equilibrium density of susceptible hosts must remain $S^* = [ln(\lambda) - ln(1-g)]/\mu$. The unstructured pathogen invades from rarity if:

$$\Re_0 = S^* (1 - e^{-\beta_0}) \nu_{\sigma,0} / (1 - \xi_0) > 1 \tag{C.5}$$

Figure 13 shows bifurcation diagrams for the unstructured-pathogen model's three state

364 variables. Parameter values match mean parameters from Fig. 15. As host natality

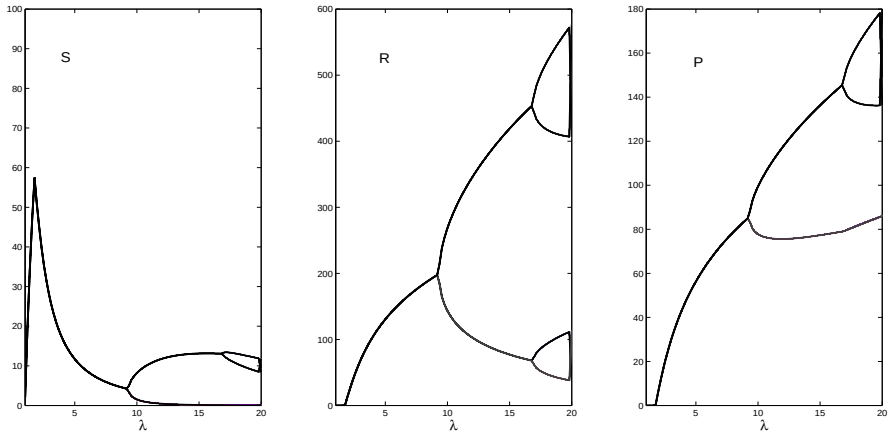

Figure 13: Bifurcation plot: low virulence in unstructured model. S, R and P are, respectively, numbers of susceptible hosts, resistant hosts, and unstructured pathogen patches. Parameters derived for unstructured dynamics from those in Fig. 15. $\nu_{\sigma,0} = 0.6$, $\nu_{\rho,0} = 0.3$, $\beta_0 = 0.12$ and $\xi_0 = 0.4$

increases, the unstructured model's equilibria include fewer susceptible and more resistant hosts. Differences in host numbers (between structured and unstructured dynamics) are, to some extent, explained by an increase in the mean total number of infectious patches in the unstructured model.

D Structured virulence: Does resistance loss matter?

Here we ask if virulence structure δ_ν interacts with the proportional loss of resistance among the R_t hosts surviving the dry season. Figure (14) shows responses of total host number ($S^* + R^*$), frequency of resistance among hosts, and numbers of stage-1 patches (all at internal equilibrium) as δ_ν increases. We iterated the computation across levels of γ.

Increased virulence structure decreases the total number of hosts, increases the proportion of hosts with resistance, and increases the equilibrium number of infectious patches. Increasing γ, the proportional loss of resistance during the dry season, has little effect on either host numbers or infectious-patch numbers. Increasing γ can produce a small

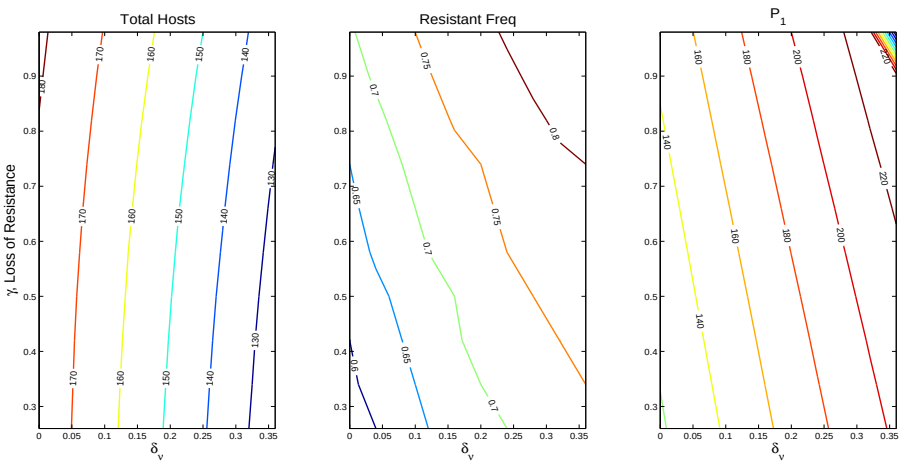

Figure 14: Virulence structure and loss of resistance. Left plot contours: $(S^* + R^*)$; center plot contours: $R^*/(S^* + R^*)$; right plot contours: P_1. Parameters: $\lambda = 5$, $g = 0.5$, $\mu = 0.01$; $\beta_1 = 0.02$, $\beta_2 = 0.01$; $\xi_1 = \xi_2 = 0.5$, $q_{21} = 0.25$; $\nu_{\rho,1} = 0.2$, $\nu_{\rho,2} = 0.1$; $\nu_{\sigma,1} = 0.5 + \delta_\nu$, $\nu_{\sigma,2} = 0.5 - \delta_\nu$.

increase in the frequency of resistance.

Increased virulence of stage-1 patches elevates disease mortality, so that the number of hosts declines, and stage-1 patches increase in number. The simultaneous decrease in virulence of stage-2 patches (which also increase in number as δ_ν increases) contributes to an increased frequency of resistance among hosts.

The unstructured equivalent to the above has $\delta_\nu = 0$, and $\beta_0 = 0.015$. Hence its interior equilibria will fall close to solutions along the ordinate of each plot. In the absence of patch structure, hosts are more numerous. Infectious patches are less numerous, and the frequency of resistance among hosts also declines when the pathogen lacks structure.

E Virulence and dynamic complexity

In a model combining standard SIR dynamics within host generations and between-generation, density-independent host growth, Koella and Doebeli [1999] numerically varied the virulence of an environmentally transmitted infection. They found

that very small changes in the frequency of lethal infection could produce qualitative changes in the host-population dynamics. Overall, their computations suggest that increasing virulence (over a narrow range) increases dynamic complexity. That is, the emergence of chaos across growth rates increased as virulence increased - for a host regulated only by disease [Koella and Doebeli 1999].

Our model's assumptions differ, as does the general effect of increased virulence on the dynamics. Figure 15 shows bifurcation plots for the four state variables at comparatively low frequencies of mortal infection. Note that in this plot, and several following, we scale the state variables differently to show the dynamics clearly. Increasing host natality leads to a series of period-doubling bifurcations in each count. Figure 16 shows that a large increase in virulence levels simplifies that dynamics over the same range of natality levels. High virulence increases the loss of susceptibles during the wet season; fewer total hosts then remain to reproduce during the dry season. Low virulence can permit the total number of hosts to advance to levels where overcompensation (*via* the Ricker term) increases dynamic complexity. That is, virulent disease can have a stabilizing effect when the host population dynamics exhibits overcompensation.

References

[Alizon and Michalakis 2015] Alizon, S., and Y. Michalakis. 2015. Adaptive virulence evolution: the good old fitness-based approach. Trends in Ecology & Evolution 30:248–254.

[Avilés 1999] Avilés, L. 1999. Cooperation and non-linear dynamics: an ecological perspective on the evolution of sociality. Evolutionary Ecology Research 1:459–467.

[Bagamian et al. 2013] Bagamian, K.H., K.A. Alexander, T.L. Hadfield, and J.K. Blackburn. 2013. Ante- and postmortem diagnostic techniques for anthrax: rethinking pathogen

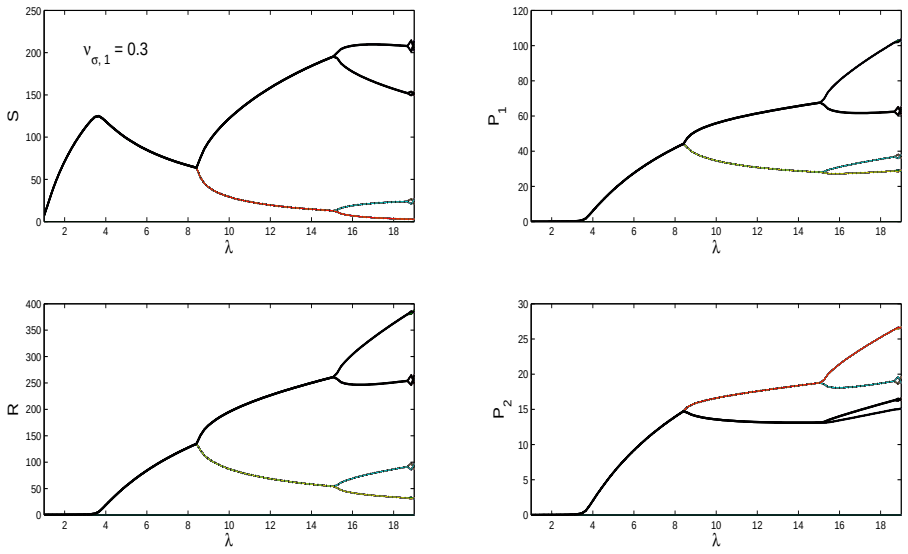

Figure 15: Bifurcation plot: low virulence. Equilibrium numbers for each state variable (see abscissa labels) as natality λ increases. $\mu = 0.01$, $g = 0.02$, $\gamma = 0.6$, $\beta_1 = 0.08$, $beta_2 = 0.04$, $\xi_1 = \xi_2 = 0.4$, $q_{12} = 0.5$ for each map. $\nu_{\sigma,1} = 0.3$, $\nu_{\sigma,2} = 0.1$, $\nu_{\rho,1} = 0.15$, and $\nu_{\rho,2} = 0.05$ for each map. For stable periodic dynamics, susceptible hosts, resistant hosts and stage-1 patches cycle together; stage-2 patches cycle "out of phase."

414 exposure and the geographic extent of the disease in wildlife. J. Wildlife Diseases 49:786–801.

416 [Bani-Yaghoub et al. 2008] Bani-Yaghoub, M., R. Gautam, Z. Shuai, P. van den Driessche, and R. Ivanek. 2008. Reproduction numbers for infections with free-living pathogens 418 growing in the environment. J. Biol. Dynamics 6:923–940.

[Breban et al. 2010] Breban, R., J.M. Drake, and P. Rohani. 2010. A general multi-strain 420 model with environmental transmission: invasion conditions for the disease-free and endemic states. J. Theor. Biol. 264:729–736.

422 [Breban et al. 2009] Breban, R., J.M. Drake, D.E. Stallknecht, and P. Rohani. 2009. The role of environmental transmission in recurrent avian influenza epidemics. PLoS Comput. 424 Biol.5:e1000346 (11 pp).

[Caraco et al. 2016] Caraco, T., C.A. Cizauskas, and I.-N. Wang. 2016. Environmentally 426 transmitted parasites: host-jumping in a heterogeneous environment. J. Theor. Biol.

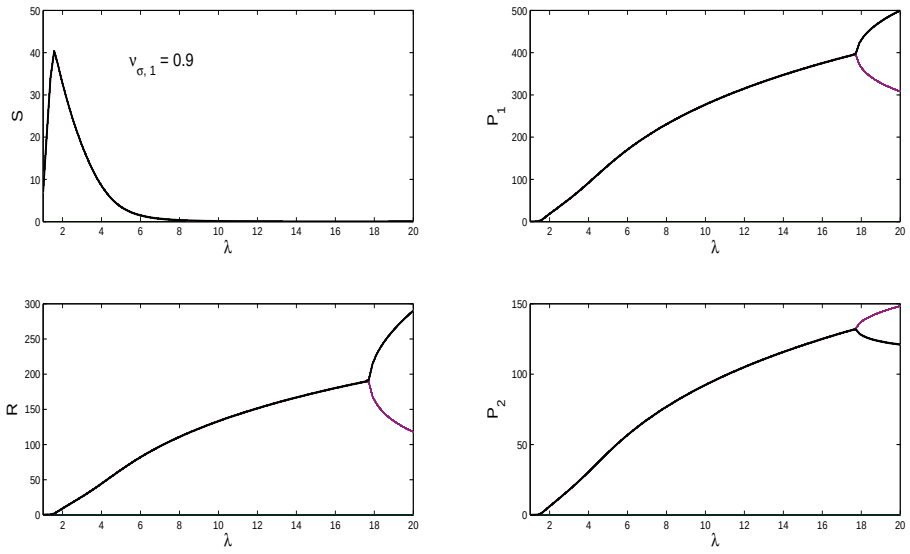

Figure 16: Bifurcation plot: high virulence. Equilibrium numbers for each state variable (see abscissa labels) as natality λ increases. Parameters same as Fig. 15, but all virulences increased. $\nu_{\sigma,1} = 0.9$, $\nu_{\sigma,2} = 0.3$, $\nu_{\rho,1} = 0.45$, and $\nu_{\rho,2} = 0.15$. Increased virulence engenders reduced dynamic complexity.

397:33–42.

[Caraco and Wang 2008] Caraco, T., and I.-N. Wang. 2008. Free-living pathogens: life-history constraints and strain competition. J. Theor. Biol. 250:569–579.

[Caraco et al. 2014] Caraco, T., A. Yousefi, and I.-N. Wang. 2014. Host-jumping, demographic stochasticity and extinction: lytic viruses. Evol. Ecol. Research 16:551–568.

[Cavalieri and Kocak 1999] Cavalieri, L., and H. Kocak. 1999. Comparative dynamics of three models for host-parasitoid interactions in a patchy environment. Bull. Math. Biol. 61:141–155.

[Cizauskas et al. 2014a] Cizauskas, C.A., S.E. Bellan, W.C. Turner, R.E. Vance, and W.M. Getz. 2014. Frequent and seasonally viable sublethal anthrax infections are accompanied by short-lived immunity in an endemic system. J. Anim. Ecol. 83:1078–1090.

[Cizauskas et al. 2014b] Cizauskas, C.A., W.C. Turner, B. Wagner, M. Küsters, R.E. Vance, and W.M. Getz. 2014. Gastrointestinal helminths may affect host susceptibility to an-

thrax through seasonal immune trade-offs. BMC Ecol. 14:27 (15 pp).

[Cressler et al. 2015] Cressler, C.E., D.W. McLeod, C. Rozins, J. Van den Hoogen, and T. Day. 2015. The adaptive evolution of virulence: a review of theoretical predictions and empirical tests. Parasitology, 16. http://doi:10.1017/S003118201500092X (16 pp).

[Day 2002] Day, T. 2002. Virulence evolution via host exploitation and toxin production in spore-producing pathogens. Ecol. Lett. 5:471–476.

[Duryea et al. 1999] Duryea, M., T. Caraco, G. Gardner, W. Maniatty, and B.K. Szymanski. 1999 Population dispersion and equilibrium infection frequency in a spatial epidemic. Physica D 132:569–579.

[Dwyer 1992] Dwyer, G. 1992. On the spatial spread of insect viruses: theory and experiment. Ecology 73:479–494.

[Dwyer 1994] Dwyer, G. 1994. Density dependence and spatial structure in the dynamics of insect pathogens. Am. Nat. 143:533–562.

[Ebert and Herre 1996] Ebert, D., and E.A. Herre. 1996. The evolution of parasitic diseases. Parasitology Today 12:96–100.

[Friedman and Yakubu 2013] Friedman, A, and A.-A. Yakubu. 2013. Anthrax epizootic and migration: persistence or extinction. Math. Biosci. 241:137–144.

[Gandon 1998] Gandon, S. 1998. The curse of the pharaoh hypothesis. Proc. R. Soc. Lond. B 265:1545–1552.

[Gasaway et al. 1996] Gasaway, W.C., K.T. Gasaway, and H.H. Berry. 1996. Persistent low densities of plains ungulates in Etosha National Park, Namibia: testing the food-regulation hypothesis. Can. J. Zool. 74:1556–1572.

462 [Godfray et al. 1997] Godfray, H.C.J., D.R. O'Reilly, and C.J. Briggs. 1997. A model of Nucleopolyhedrovirus (NPV) population genetics applied to co-occlusion and the spread of
464 the few polyhedra (FP) phenotype. Proc. R. Soc. Lond. B 264:315–322.

[Havarua et al. 2014] Havarua, Z., W.C. Turner, and J.K.E. Mfune. 2014. Seasonal variation
466 in foraging behavior of plains zebras (*Equus quagga*) may alter contact with the anthrax bacterium (*Bacillus anthracis*). Canadian J. Zoology 92:331–337.

468 [Kaitala et al. 1999] Kaitala, V., J. Ylikarjula, and M. Heino. 1999. Dynamic complexities in host-parasitoid interaction. J. Theor. Biol. 197:331–341.

470 [Kaplan and Glass 1995] Kaplan, D., and L. Glass. 1995. Understanding Nonlinear Dynamics. Springer-Verlag, New York USA.

472 [Koella and Doebeli 1999] Koella, J.C., and M. Doebeli. 1999. Population dynamics and the evolution of virulence in epidemiological models with discrete host generations. J. Theor.
474 Biol. 198:461–475.

[May et al. 1981] May, R.M., M.P. Hassell, R.M. Anderson, and D.W. Tonkyn. 1981. Density
476 dependence in host-parasitoid models. J. Anim. Ecol. 50:855–865.

[Miller et al. 2006] Miller, M.W., N.T. Hobbs, and S.T. Tavener. 2006. Dynamics of prion
478 disease transmission in mule deer. Ecol. Appl. 16:2208–2214.

[Moore et al. 2014] Moore, S.M., K.L. Shannon, C.E. Zelaya, A.S. Azman, and J. Lessler.
480 2014. Epidemic risk from cholera introductions into Mexico. PLoS Currents: Outbreaks. doi:10.137/currents.outbreaks.c04478c7fbd9854ef6ba923cc81eb799. (17 pp).

482 [Neubert and Kot 1992] Neubert, M.G., and M. Kot. 1992. The subcritical collapse of predator populations in discrete-time predator-prey models. Mathematical Biosciences 110:45–
484 66.

[Reeson et al. 2000] Reeson, A.F., K. Wilson, J.S. Cory, P. Hankard, J.M. Weeks, D. Goulson, and R.S. Hails. 2000. Effects of phenotypic plasticity on pathogen transmission in the field in a Lepidoptera-NPV system. Oecologia 124:373–380.

[Rijks 1999] Rijks, J. 1999. A serological study of bison (*Bison bison*) in an area of northern Canada experiencing sporadic and epizootic anthrax. University of London, London UK.

[Roche et al. 2011] Roche, B., J.M. Drake, and P. Rohani. 2011. The curse of the pharaoh revisited: evolutionary bi-stability in environmentally transmitted pathogens. Ecol. Lett. doi: 10.1111/j.1461-0248.2011.01619.x (7 pp).

[Rohani et al. 2009] Rohani, P., R. Breban, D.E. Stallknecht, and J.M. Drake. 2009. Environmental transmission of low pathogenicity avian influenza viruses and its implications for pathogen invasion. PNAS 106:10365–10369.

[Ross 1983] Ross, S.M. 1983. Stochastic processes. John Wiley & Sons, New York.

[Ruxton and Rohani 1998] Ruxton, G.D., and P. Rohani. 1998. Population floors and the persistence of chaos in ecological models. Theor. Pop. Biol. 53:175–183.

[Trainor and Caraco 2006] Trainor, K.T. and T. Caraco. 2006. Group size, energy budgets, and population dynamic complexity. Evolutionary Ecology Research 8:1173–1192.

[Turnbull 2008] Turnbull, P.C.B. 2008. *Anthrax in humans and animals*. 4th Edit. Geneva, Switzerland. World Health Organization.

[Turner et al. 2006] Turner, J., R.G. Bowers, M. Begon, S.E. Robinson, N.P. French. 2006. A semi-stochastic model of the transmission of Escherichia coli O157 in a typical UK dairy herd: Dynamics, sensitivity analysis and intervention/prevention strategies. J. Theor. Biol. 241:806–822.

[Turner et al. 2013] Turner, W.C., P. Imologhome, Z. Havarua, G.P. Kaaya, J.K.E. Mfune, I.D.T. Mpofu, and W.M. Getz. 2013. Soil ingestion, nutrition, and the seasonality of anthrax in herbivores of Etosha National Park. Ecosphere 4:13 (19 pp).

[Turner et al. 2016] Turner, W.C., K.L. Kausrud, W. Beyer, et al. 2016. Lethal exposure: An integrated approach to pathogen transmission via environmental reservoirs. Sci. Reports 6:27311 (13 pp).

[Turner et al. 2014] Turner, W.C., K.L. Kausrud, Y.S. Krishnappa, J.P.G.M. Cromsigt, H.H. Ganz, I. Mapaure, C.C. Cloete, Z. Havarua, M. Küsters, W.M. Getz, and N.C. Stenseth. 2014. Fatal attraction: vegetation responses to nutrient inputs attract herbivores to infectious anthrax carcass sites. Proc. Roy. Soc. B 281:20141785 (9 pp).

[Walther and Ewald 2004] Walther, B., and P.W. Ewald. 2004. Pathogen survival in the external environment and the evolution of virulence. Biol. Rev. Camb. Philos. Soc. 79:849 – 869.